INDUSTRIAL ROBOTS

The milliDelta: A high-bandwidth, high-precision, millimeter-scale Delta robot

Hayley McClintock,[1]*† Fatma Zeynep Temel,[1]*† Neel Doshi,[1] Je-sung Koh,[1,2] Robert J. Wood[1]†

Delta robots have been widely used in industrial contexts for pick-and-place applications because of their high precision and speed. These qualities are also desirable at the millimeter scale for applications such as vibration cancellation in microsurgery and microassembly or micromanipulation. Developing a millimeter-scale Delta robot that maintains the characteristic input-output behavior and operates with high speed and precision requires overcoming manufacturing and actuation challenges. We present the design, fabrication, and characterization of an adapted Delta robot at the millimeter scale (the "milliDelta") that leverages printed circuit microelectromechanical system manufacturing techniques and is driven by three independently controlled piezoelectric bending actuators. We validated the design of the milliDelta, where two nonintersecting perpendicular revolute joints were used to replace an ideal universal joint. In addition, a transmission linkage system for actuation was introduced to the laminate structure of the milliDelta. This 15 millimeter–by–15 millimeter–by–20 millimeter robot has a total mass of 430 milligrams and a payload capacity of 1.31 grams and operates with precision down to ~5 micrometers in a 7.01-cubic-millimeter workspace. In addition, the milliDelta can follow periodic trajectories at frequencies up to 75 hertz, experiencing velocities of ~0.45 meters per second and accelerations of ~215 meters per squared second. We demonstrate its potential utility for high-bandwidth, high-precision applications that require a compact design.

INTRODUCTION

Parallel manipulators exhibit many favorable characteristics, including high speeds and accelerations, low inertias, high stiffnesses, and superior precision relative to serial manipulators (*1*–*3*). In 1990, Clavel (*4*–*6*) introduced the Delta robot: a 3-DOF (degrees of freedom) parallel mechanism motivated by the need for a pick-and-place tool in a chocolate factory (*7*). In addition to the traditional advantages of parallel manipulators, the Delta robot provides decoupling between the orientation and translation of the end effector (*3*–*6*) and has simple closed-form kinematic solutions (*1*, *6*, *8*, *9*). This is a marked improvement over earlier parallel mechanism designs, which suffered from limited workspaces, complicated mechanical design, and complex kinematics (*3*, *6*, *10*, *11*). For these reasons, Delta robots are widely used in industrial applications, such as food packaging, machining, welding, and pick-and-place assembly (*2*, *3*, *6*, *12*). The advantages of the Delta robot design, including a low inertia that allows for high speed and acceleration, improve as size decreases, making the design desirable for small-scale applications such as microassembly, micromanipulation, and medical robotics (*13*–*16*). For these applications, there has been development in the design and fabrication of Delta robots with workspaces tailored to this scale (*13*–*18*). These robots demonstrate the scalability of the Delta robot design but are still at the mesoscale (~10 cm). Whereas these designs often couple traditional manufacturing techniques (*13*, *14*, *19*) with novel flexure design (*14*, *16*, *18*), an integrated approach to design and fabrication must be used to achieve a millimeter-scale Delta robot for better incorporation into devices, such as surgical tools, as an end effector.

For developing robots at the millimeter scale, smart composite microstructures and printed circuit microelectromechanical systems (PC-MEMS) enable the fabrication of highly articulated three-dimensional (3D) structures (*20*–*23*). By leveraging these design and fabrication techniques, high-performance composite materials, and zero-backlash flexural joints, we can realize complex mechanisms, such as those found in parallel manipulators, at the millimeter scale. Using a laminate structure also yields advantages such as scalability, reduced cost, and improved performance (*24*). For example, dimensional parameters can easily be adjusted for meso- to microscale applications. Last, millimeter-scale laminate structures require less maintenance than traditionally manufactured devices as a result of fewer moving parts (*24*).

Various actuators exist at the millimeter scale, including rotary motors (*25*), soft microactuators (*26*, *27*), voice coil actuators (*18*, *25*), and piezoelectric actuators (*25*, *28*–*30*). However, rotary motors function poorly because of surface effects (*16*, *25*, *31*), microfluidic actuators are limited in their maximum operational frequency (*26*), and voice coil actuators require suspension (*18*, *25*). Because of their high (kilohertz) bandwidth, high power density, and low profile, piezoelectric bending actuators are well suited to power motion in millimeter-scale devices (*28*–*30*, *32*–*34*). Using piezoelectric actuators enables devices to be scaled down significantly and increases their maximum operational frequency.

We present the milliDelta, a 15 mm–by–15 mm–by–20 mm Delta robot (Fig. 1) based on the PC-MEMS manufacturing technique and driven by piezoelectric bending actuators. We modified the design of the conventional Delta robot for monolithic fabrication and developed custom fixtures for improved assembly and actuator integration. These modifications were validated, and the characterization of the milliDelta's workspace, payload capacity, bandwidth, precision, and accuracy is described in the Results. The milliDelta has a mass of 430 mg (60-mg linkage mass and 370-mg actuator mass) and achieves a maximum workspace of 7.01 mm^3 with a payload capacity of 1.31 g (~3 times its mass). In addition, piezoelectric bending actuators enable operation at frequencies up to 75 Hz, which, to the best of the authors' knowledge, is 15 to 25 times higher bandwidth than that of currently available Delta robots (*35*) (Table 1).

The scalability and small size of the milliDelta make it a good candidate to replace bulky mechanical structures in millimeter-scale robotic applications that require high precision and accuracy, including micropositioning stages, novel wrist mechanisms for robotic arms,

[1]John A. Paulson School of Engineering and Applied Sciences and Wyss Institute for Biologically Inspired Engineering, Harvard University, Cambridge, MA 02138, USA. [2]Department of Mechanical Engineering, Ajou University, Suwon, South Korea.
*These authors contributed equally to this work.
†Corresponding author. Email: hayley.mcclintock@wyss.harvard.edu (H.M.); fztemel@seas.harvard.edu (F.Z.T.); rjwood@seas.harvard.edu (R.J.W.)

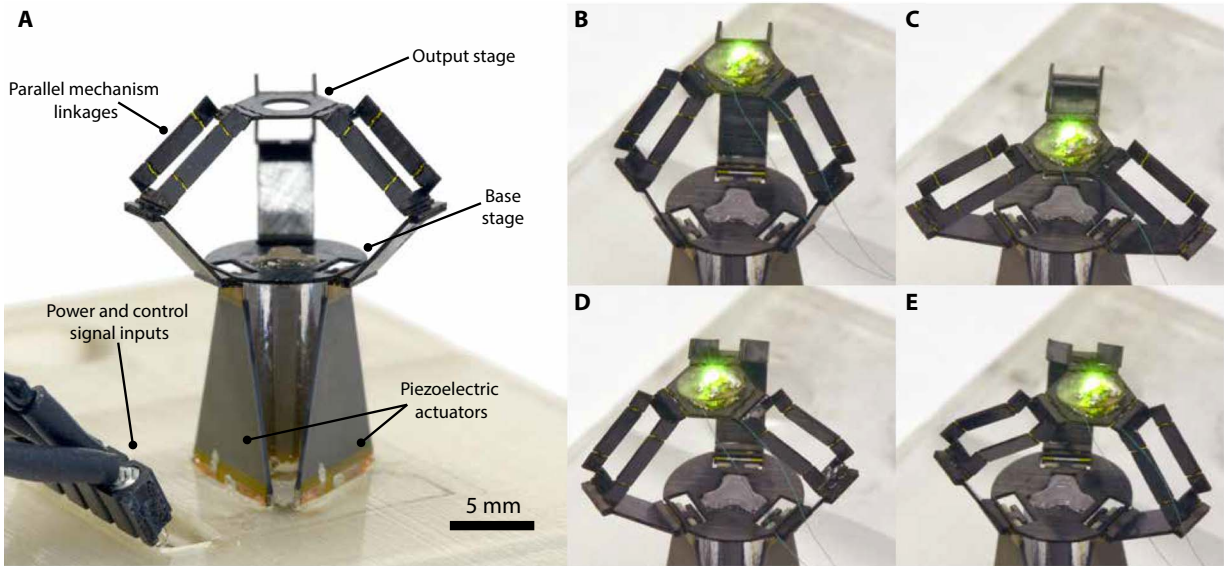

Fig. 1. The milliDelta: a millimeter-scale Delta robot. Design of the milliDelta is based on origami-inspired engineering and made using PC-MEMS manufacturing techniques. The robot is driven by three piezoelectric bending actuators. Power and control signals were delivered via a five-wire tether. (**A**) The milliDelta with components labeled. Perspective views of the milliDelta moving through its workspace near the top (**B**), bottom (**C**), left (**D**), and right (**E**) with externally powered light-emitting diode for visualization.

Table 1. Relevant parameters for a selection of currently available Delta robots.

Device	Size (mm)	Weight (g)	Workspace (mm^3)	Frequency (Hz)	Payload (N)	Accuracy (μm)
IRB 360 FlexPicker (*35*)	565 radius 1000 height	120,000	~3.5×10^8	~3	~78	100
Adept Quattro s650HS (*35*)	650 radius 1150 height	117,000	~6.6×10^8	5	~59	100
Pocket Delta (*35*)	171 × 171 × 270	5.6	~4.8×10^5	2	0.2	3
Laminated Delta robot (*16*)	~100 ×100 ×100	—	~700	—	1	100
milliDelta	15 × 15 × 20	0.430	7.01	75	0.0131	5

and micromanipulation and microscale pick-and-place applications. We demonstrated the robot's precision [~5-μm root mean square (RMS)] when tracking complex trajectories and performing high-speed motions. Although other micromanipulators developed at this scale are precise down to 0.1 μm, these devices are unable to reach frequencies as high as the milliDelta (*14*, *15*, *36*), which enables rapid automation in microassembly tasks and microfabrication systems. In addition, because of reduced cost from miniaturization, the milliDelta can be used as an (potentially disposable) end effector in medical devices. For example, the milliDelta can be used for tremor compensation, and we showed its ability to reduce hand tremors by 81%. This reduction is comparable to that of similar, fully integrated vibration cancellation devices (also between 80 and 90%) (*37*) and table-top surgical systems (*38*) and close to that of surgical robots teleoperated by surgeons (*39*).

RESULTS

Design

Conventional Delta robots consist of two parallel plates—the fixed base and the moving output stage—connected by three kinematic chains (*2*, *7*, *40*). Each chain is driven by a single-DOF actuator connected to the fixed base. The base arm linkage transmits the motion to two parallel bars that are connected to the output stage. These parallel bars form a parallelogram structure that is key for the functionality of the Delta robot (*7*). The joints between the base arm linkage, parallelogram, and the output stage are universal joints.

The milliDelta (Fig. 2) was designed using a 3D computer-aided design (CAD) software (SolidWorks) and custom laminate design software (popupCAD) (*41*). The rotational joints at the fixed base of the Delta robot were replaced with revolute flexural joints, with an inherent stiffness and damping (*42*). Each of the six universal joints was separated into two perpendicular revolute flexural joints, as shown in Fig. 2D. The perpendicular revolute joints provide 2-DOF rotation about two perpendicular axes, approximating a universal joint as discussed in Design verification. Furthermore, assembly flexural joints fixed at an angle of 45° are introduced to keep the moving flexural joints unloaded at the center of the milliDelta's workspace (fig. S2C).

Three additional input linkages, crank sliders in series with a linearizing revolute flexural joint, as described in (*43*), were added to the milliDelta (Fig. 2, A to C). These transmissions convert and amplify

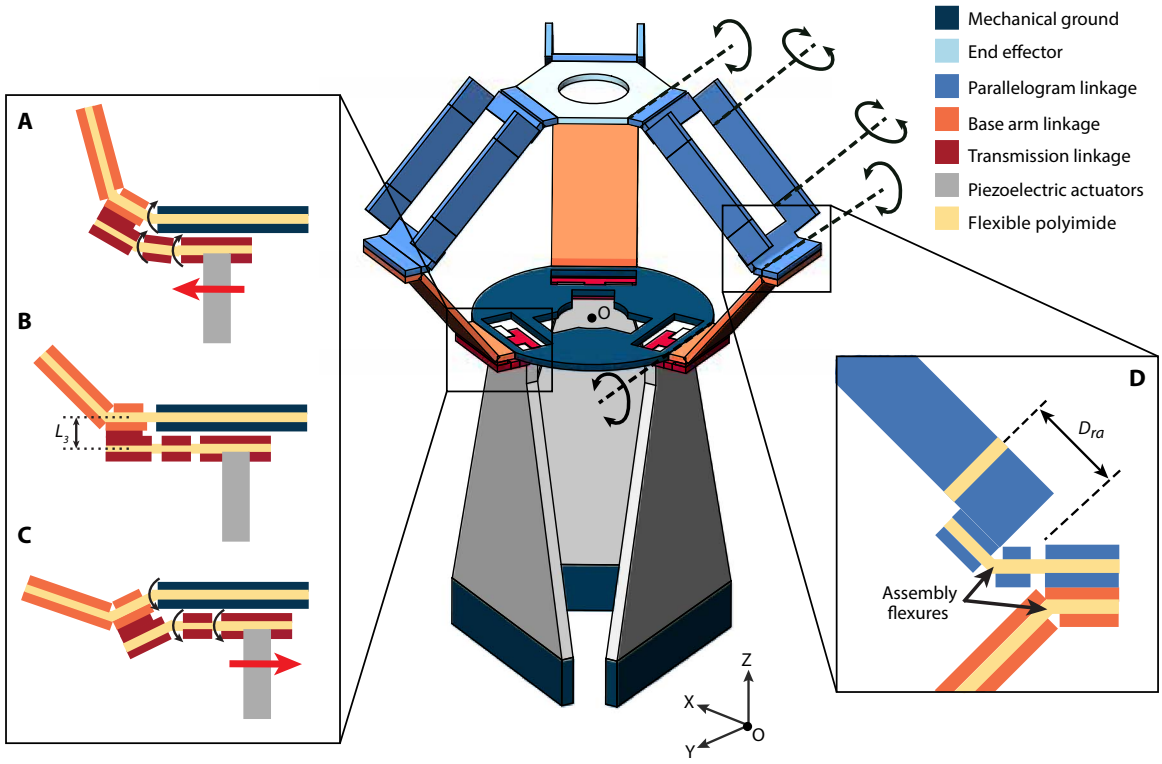

Fig. 2. Schematic representation of the milliDelta. Revolute joint axes are labeled with dashed black lines. The composite laminate structure is shown with mechanical components as described in the legend. The milliDelta has two parallel plates (the fixed base and the output stage) that are connected by three kinematic chains, each consisting of base arm and parallelogram linkages. Three additional input transmission linkages were added to convert and amplify (by $1/L_3$) the bending motion (red arrow) of the actuators to rotary motion at the fixed base (black arrow). Cross-sectional views of input transmission linkages are shown in upper (**A**), neutral (**B**), and lower (**C**) configurations with flexible polyimide layer as shown in the legend. (**D**) Universal joints conventionally present at the fixed base and at the output stage were approximated with two perpendicular revolute joints separated by distance D_{ra}. Assembly flexural joints fixed at an angle of 45° were introduced to keep the moving flexural joints unloaded at the center of the milliDelta's workspace.

the bending input motion of the piezoelectric actuators to a rotary motion of the revolute flexural joints at the fixed base. The amplification (transmission ratio) is determined by $1/L_3$ (length L_3 is labeled in Fig. 2B and fig. S1). Piezoelectric bending actuators can be modeled as a force source proportional to the magnitude of the input voltage in parallel with a nonlinear spring (*28*). The peak-to-peak input voltage and the actuator tip deflection were limited to ~225 V (1.7 μm/V field) and ~600 μm, respectively, to increase lifetime (*28*). Given these considerations, the models presented in (*28*) and (*43*) were used in an iterative experimental procedure to determine input linkage lengths, actuator dimensions, and flexural stiffnesses to achieve about ±45° of rotation (see table S1 and fig. S1).

Design verification

Ideal universal joints, as found in conventional Delta robots, can be realized for laminate manufacturing by using a spherical five-bar linkage system with two coincident rotational axes (*44*). However, the complexity of this linkage system can introduce manufacturing errors in small-scale devices, specifically when manual assembly is required. To reduce this error in the design of the milliDelta, we used two perpendicular revolute joints with offset axes of rotation to approximate ideal universal joints (Fig. 2D).

To understand the effect of this axis bias on the motion of the milliDelta's output stage, we performed a simulation study using the kinematic model described in Materials and Methods. For this study, three workspaces are calculated using different bias distances between the rotational axes of the approximated universal joints, D_{ra} (Fig. 2D). The milliDelta has a D_{ra} of 0.8 mm. Its workspace was compared to that of a conventional Delta robot (D_{ra} = 0 mm) and a two times bias case (D_{ra} = 1.6 mm), with all other dimensional parameters and inputs kept constant (Fig. 3). As D_{ra} increased, an anisotropic change occured in the workspace: The coverage decreased in the *xy* plane and increased in the *xz* plane. Using actuator input deflections of ±70 μm, the workspace volumes of the conventional design, the milliDelta, and the two times bias case were calculated as 7.30 mm^3, 7.17 mm^3, and 7.86 mm^3, respectively. These deviations are relatively minor (7.5%), demonstrating that two nonintersecting perpendicular revolute joints can be used to replace an ideal universal joint in manufacturing microrobots with PC-MEMS techniques.

Quasi-static characterization

Workspace measurements

We performed an experimental characterization of the milliDelta's workspace by recording the position of its output stage for various inputs. Eighteen actuation schemes were tested to determine the extent of the milliDelta's workspace (Fig. 4). While performing these workspace motions, the milliDelta exhibited an average RMS deviation from the mean trajectory of 4.6 ± 0.9 μm (n = 18 trials). These trajectories are displayed (Fig. 4) alongside the kinematic model's predictions based on the average observed actuator deflection (~ ±70 μm). To calculate the total workspace of the milliDelta, we used a polynomial fit to create a 3D volume (7.01 mm^3). The experimental workspace closely

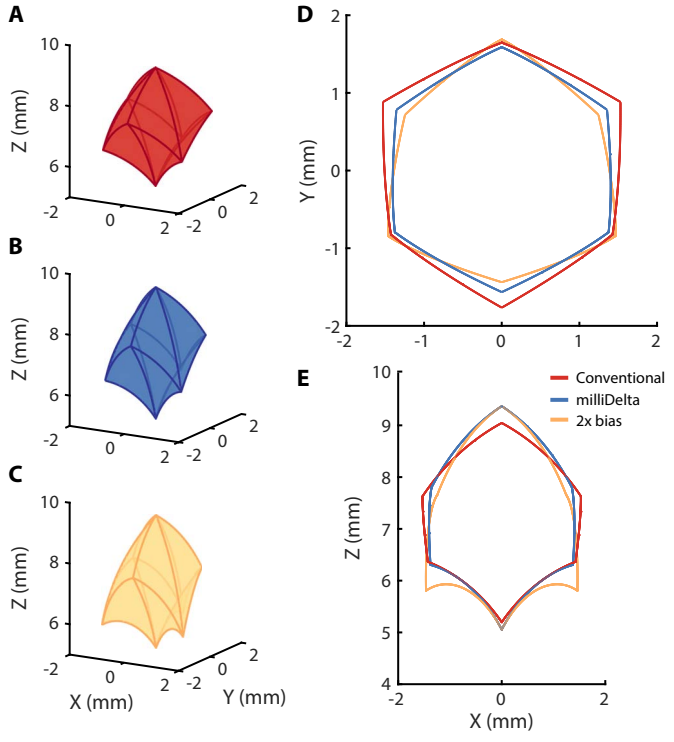

Fig. 3. Workspace comparison of Delta robots. A comparison of (**A**) a conventional Delta robot design (D_{ra} = 0 mm), (**B**) the milliDelta (D_{ra} = 0.8 mm), and (**C**) a Delta robot with 2× axis bias (D_{ra} = 1.6 mm). The *xy* projection of the workspaces is shown in (**D**), and the *xz* projection is shown in (**E**).

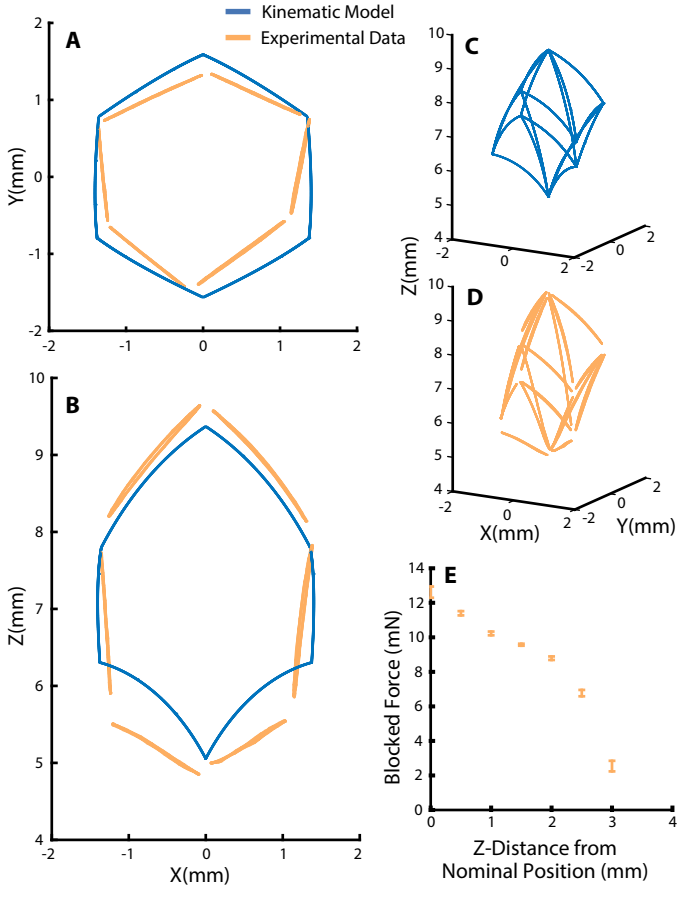

Fig. 4. Experimental characterization of the milliDelta's quasi-static workspace (yellow) compared with the theoretical workspace (blue) generated by the kinematic model. Outlines of the *xy* and *xz* projections of the workspaces are shown in (**A**) and (**B**). The 18 trajectories shown in (**C**) and (**D**) outline the extent of the workspace with actuator input amplitudes selected to avoid collision between linkages for all trajectories. (**E**) Experimental blocked force measurements in the vertical (*z*) direction as a function of vertical distance from the center of the workspace. The stiffness increased as the millDelta approached the extent of its workspace. Error bars indicate 1 SD.

matches the predicted workspace in both shape and volume. The difference between kinematic and experimental workspaces is calculated as 0.16 mm^3 (~2%) and is likely due to fabrication errors and material imperfections that cause asymmetries between arms. These discrepancies can be reduced by using pop-up fabrication to eliminate manual assembly (see Materials and Methods) and more sophisticated system identification techniques, including reinforcement learning or through the use of gray-box dynamic models that can be calibrated for an individual robot.

Force measurements

Force characterization of the milliDelta in the vertical direction was performed by using a single-axis force sensor. The peak forces at each height are shown in Fig. 4E, with a maximum measured force of 13.1 ± 0.16 mN (n = 5). The vertical stiffness of the milliDelta increased with height; it was lowest near the neutral position (z = 0 mm) and highest near the top of its workspace (z = 3.5 mm). This increase in stiffness is expected as the robot approaches a kinematic singularity at the extent of its workspace. The milliDelta's force capability is sufficient for applications such as retinal microsurgery, where 75% of forces are less than 7.5 mN in magnitude (*45*), making it suitable for use as a tremor compensating end effector.

Bandwidth characterization

The frequency response of the milliDelta is experimentally measured for small displacements (~300 μm RMS) about its neutral configuration (see Experimental setup and procedure). A continuous linear representation (Eq. 1) of the milliDelta's dynamics near its nominal position is estimated using subspace methods (*46*). The state $\boldsymbol{x}$ is prescribed to be 6D because the robot is a 3-DOF second-order dynamical system. The 3D position of the output stage is used as the output vector, $\boldsymbol{y} = (x, y, z)$, and the three drive voltages form the input vector, $\boldsymbol{u} = (V_1, V_2, V_3)$. No restrictions were placed on the matrices A, B, and C.

$$\frac{\partial \boldsymbol{x}}{\partial t} = A\boldsymbol{x} + B\boldsymbol{u}$$
$$\boldsymbol{y} = C\boldsymbol{x} \quad (1)$$

Figure 5 illustrates the magnitude response of the 3 × 3 transfer function matrix $H(j\omega)$ (Eq. 2) of the estimated linear system, where j is the imaginary unit, ω is the frequency in radians per second, and I is the 6 × 6 identity matrix. This is compared with the experimental magnitude response of the output stage with each arm actuated individually.

$$H(j\omega) = C(j\omega I - A)^{-1}B \quad (2)$$

The linear system accurately represents the experimental magnitude response in this region, with an average position error of 32 ± 1 μm

RMS (~10% of the region) computed for the three single-arm actuations. The symmetries in the milliDelta's dynamics are easily identified in the magnitude response plots; for example, all three arms have similarly shaped magnitude responses in the *z* direction. Furthermore, arms one and three are symmetric and have a similar response in all three directions. Arm two is aligned with the *x* axis and displays relatively little motion in the *y* direction.

The operational envelope of the milliDelta and the resonant modes are shown in a singular value plot of $H(j\omega)$ (fig. S3). Despite the addition of a tracking marker (~18% of the milliDelta's linkage mass), the resonant modes of this system are between 75 and 95 Hz, allowing the robot to operate at frequencies up to 75 Hz without accounting for resonant behavior.

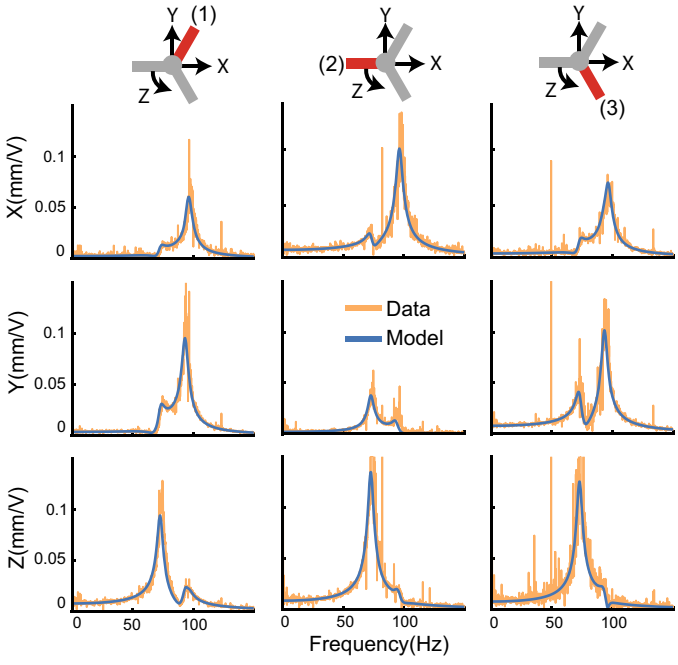

Fig. 5. Magnitude response, $|H(j\omega)|$, of the milliDelta's output stage for small perturbations in the Cartesian directions (rows) for each arm (columns). The estimated linear system is shown in blue, and experimental magnitude response is shown in orange. Resonant modes, with the addition of a tracking marker, were between 75 and 95 Hz.

DISCUSSION

Here, we present the design, modeling, fabrication, and characterization of the milliDelta (430 mg mass, 15 mm × 15 mm × 20 mm size) driven by piezoelectric bending actuators. The milliDelta can achieve high precision at frequencies 15 to 25 times higher than currently available Delta robots without complex sensing and control, which is difficult to implement at the millimeter scale. More generally, the milliDelta illustrates that mechanisms found in conventional Delta robots can be realized at the millimeter scale by using laminate design, PC-MEMS techniques, assembly scaffolds, and high power density actuators. These design and fabrication choices and the use of high-performance composite materials result in a compact device that improves on the advantages of conventional Delta robots, including high precision and bandwidth.

To demonstrate the milliDelta's ability to perform complex trajectories necessary for micromanipulation and microscale pick and place, we used the kinematic model to generate input signals for planar circle, star, and H trajectories (Fig. 6 and movie S2) at 1 Hz. The robot's motion was compared with the desired output, and the precision and accuracy across cycles ($n = 5$) is tabulated in Table 2. At low frequencies, the milliDelta was able to repeat trajectories with an average RMS deviation from the mean trajectory (RMS precision) down to 1.9 ± 0.5 μm ($n = 5$). Furthermore, an average RMS deviation from the desired trajectory (RMS accuracy) as low as 24.7 ± 0.2 μm ($n = 5$) was achieved. The small-deflection linear dynamic model (see Bandwidth characterization) was inverted to allow the robot to create a star trajectory at 20 Hz with an RMS accuracy of 68.6 ± 0.4 μm ($n = 5$) and an RMS precision of 5.2 ± 0.9 μm ($n = 5$). These values demonstrates the milliDelta's ability to perform motions necessary for pick and place at a frequency higher than those of currently available Delta robots. For smooth motions, it can operate at even higher frequencies and can create a planar 1.5-mm-diameter circle at its lowest resonant frequency of 75 Hz (Fig. 6E and movie S1). The output stage moved with a linear velocity of ~0.45 m/s and experienced accelerations of ~215 m/s^2 (~22*g*) while tracing this circle. The RMS accuracy for this high-frequency trajectory decreased to 211.9 ± 1.4 μm ($n = 5$),

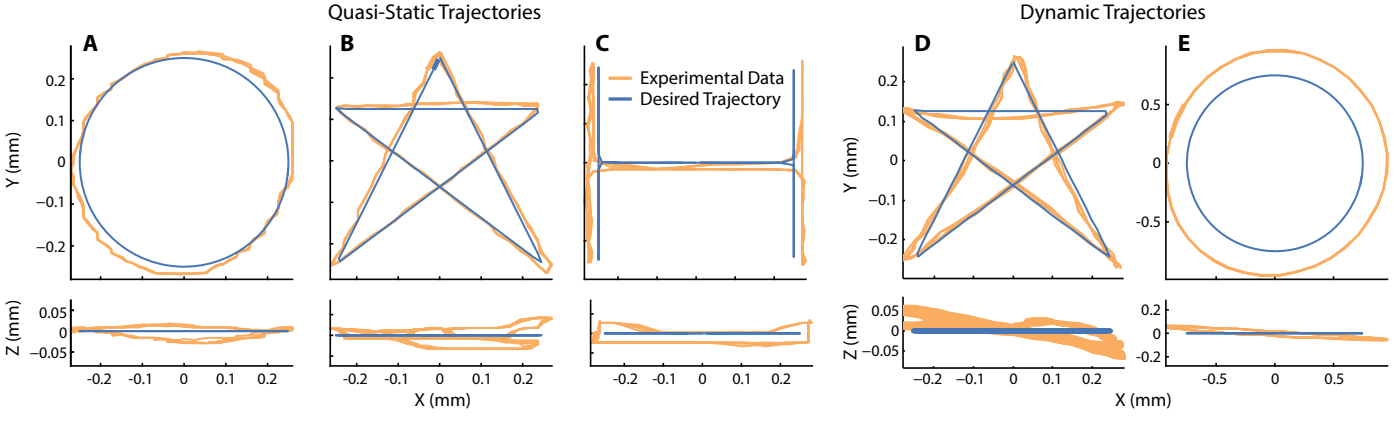

Fig. 6. Quasi-static and dynamic trajectories. Left: Quasi-static (1 Hz) experimental (orange) and desired (blue) trajectories for a 0.5-mm-length planar circle (**A**), star (**B**), and H (**C**). Control inputs were determined by using the kinematic model. Right: High-bandwidth experimental (orange) and desired (blue) trajectories for a 0.5-mm-length star executed at 20 Hz (**D**) and a 1.5-mm-diameter circle executed at 75 Hz (**E**). Control inputs were determined by using the estimated linear dynamic model.

Table 2. Trajectory following results. RMS precision and accuracy are calculated over five cycles of data recorded at 100 fpc.

Trajectory	Frequency (Hz)	Length (μm)	RMS precision (μm)	RMS accuracy (μm)
Circle	1	500	2.3 ± 1.1	34.9 ± 0.1
Star	1	500	1.9 ± 0.5	24.7 ± 0.2
H	1	500	2.4 ± 0.8	33.2 ± 0.2
Star	20	500	5.2 ± 0.9	68.6 ± 0.4
Circle	75	1500	4.3 ± 1.4	211.9 ± 1.4

but an RMS precision of 4.3 ± 1.4 μm (n = 5) was maintained. This degradation in accuracy is due to the failure of the linear model to capture the nonlinear dynamics that manifest themselves, as the output stage moves away from its neutral position. Overall, the milliDelta's ability to follow given trajectories at increasing frequencies with high RMS precision and accuracy establishes its utility for micromanipulation tasks.

Leveraging the milliDelta's high precision and bandwidth, we also demonstrated its potential for tremor compensation in surgical or assembly operations (see movie S3). Typical hand tremors range from ~8 to 12 Hz and are 50 μm peak to peak in each of the principal axes (*47*–*50*), which falls well within the milliDelta's operational envelope. Hand tremors were measured for three individuals (two shown in Fig. 7 and movie S3 for clarity) attempting to hold a visual marker in place. The estimated linear model was inverted offline to determine the input trajectory that allows the robot to track the hand tremors. The resulting motion of the milliDelta was recorded and the tracking error was computed. The RMS tracking error averaged over all three individuals is 81 ± 4% smaller than the RMS tremor amplitude, which demonstrates the milliDelta's ability to successfully mitigate hand tremors. In addition, the robot's small form factor and low mass make it a suitable end effector for existing devices.

The design of the milliDelta can also be further optimized for tremor mitigation or micromanipulation. For example, the smaller workspace required for tremor mitigation would allow for a significantly lower transmission ratio, improving payload capacity and reducing the robot's size and mass. The current mounting system can also be easily modified for incorporation with existing devices. Alternatively, the linkages and actuators can be redesigned to increase the workspace for micromanipulation tasks. Using the design and fabrication methodology described here, the milliDelta can be reconfigured for an application with specific design requirements (that is, workspace, precision, bandwidth, and payload). Overall, the milliDelta demonstrates the advantages of scaling down parallel mechanisms, and the PC-MEMS process combined with the use of high power density actuators can be applied to other parallel manipulators for high performance at small scales.

MATERIALS AND METHODS

Kinematic model

The milliDelta's kinematics deviate slightly from that of a conventional Delta robot because of design modifications (see Design) that enable fabrication at the millimeter scale. Consequently, the forward and inverse kinematics were computed by using MATLAB's multibody simulation environment (Simscape Multibody). Each link was modeled as shown in fig. S1 with geometric parameters (table S1) taken from the 3D CAD model. Kinematic transformations between links were defined by using a 0-DOF weld joint to represent rigid connections between links and a 1-DOF revolute joint for flexures. One-DOF prismatic joints between each transmission linkage and the world frame represent the linearized deflections of the three actuators. Loop constraints were enforced at the output stage. Inputs for forward kinematics were the actuator deflections, and the outputs were the Cartesian position of the center of the output stage. For the inverse kinematics, a 3-DOF Cartesian joint between the center of the output stage and world frame was used to input different trajectories, and the linearized actuator deflections were recorded as outputs.

Manufacturing the milliDelta

The rigid layers of the milliDelta were formed by curing three sheets of single-layer carbon fiber (Q1-112, Toho Tenax) together at orthogonal angles, yielding a final composite with a thickness of ~100 μm. A 12.5-μm polyimide film (Kapton, DuPont) was used for the flexible layers to generate the flexures, and heat- and pressure-activated sheet adhesive (Pyralux FR1500, DuPont) bonded each layer of the laminate. Each layer was individually cut by using a laser micromachining system (Oxford Lasers), as shown in fig. S2A. After each layer was cut, the carbon fiber and polyimide were ultrasonically cleaned with isopropyl alcohol, plasma-etched (Diener) for enhanced bonding, aligned laterally for lamination using precision dowel pins, and then cured together using heat and pressure (fig. S2B). The resulting laminate was laser micromachined to release the structure from the surrounding bulk material (fig. S2B). To improve assembly, we placed the milliDelta in a custom jig that fixed the linkages in the desired neutral state and constrained the moving flexures. Once in this configuration, the fixed flexures were glued to ensure that the robot was properly aligned and that the moving flexures remained unloaded in the neutral configuration (fig. S2C). This assembly fixture enabled rapid design iterations, but some assembly errors still occurred. Once a mature design was reached, a pop-up approach to fabrication (*44*) can be used to further automate folding, improve linkage alignment, and eliminate manual assembly.

Once released from the assembly scaffold, the milliDelta was attached to three piezoelectric bending actuators, which were aligned using a custom 3D-printed base (Stratasys). The pizeoelectric bending actuators were fabricated by using the materials and techniques described in (*28*) but with the substitution of 25-μm copper-clad polyimide film (Dupont) for the bridges. The 3D-printed base served as mechanical ground for the actuators and the milliDelta's base stage and housed the routing circuitry. Power and control signals were generated off-board and were delivered via a five-wire tether.

Experimental setup and procedure

The experimental setup in Fig. 8 was used to determine the workspace and frequency response, as well as to perform tremor compensation and path following. The milliDelta was fixed to a micropositioning stage (Thorlabs) and centered in the fields of view of two orthogonally positioned high-speed cameras (Phantom v7.3) with a spatial resolution of ~30 μm per pixel. The motion of the milliDelta was tracked using vision-based tracking (Xcitex-ProAnalyst) with sub-pixel accuracy. The cameras were time-synced through an xPC target system

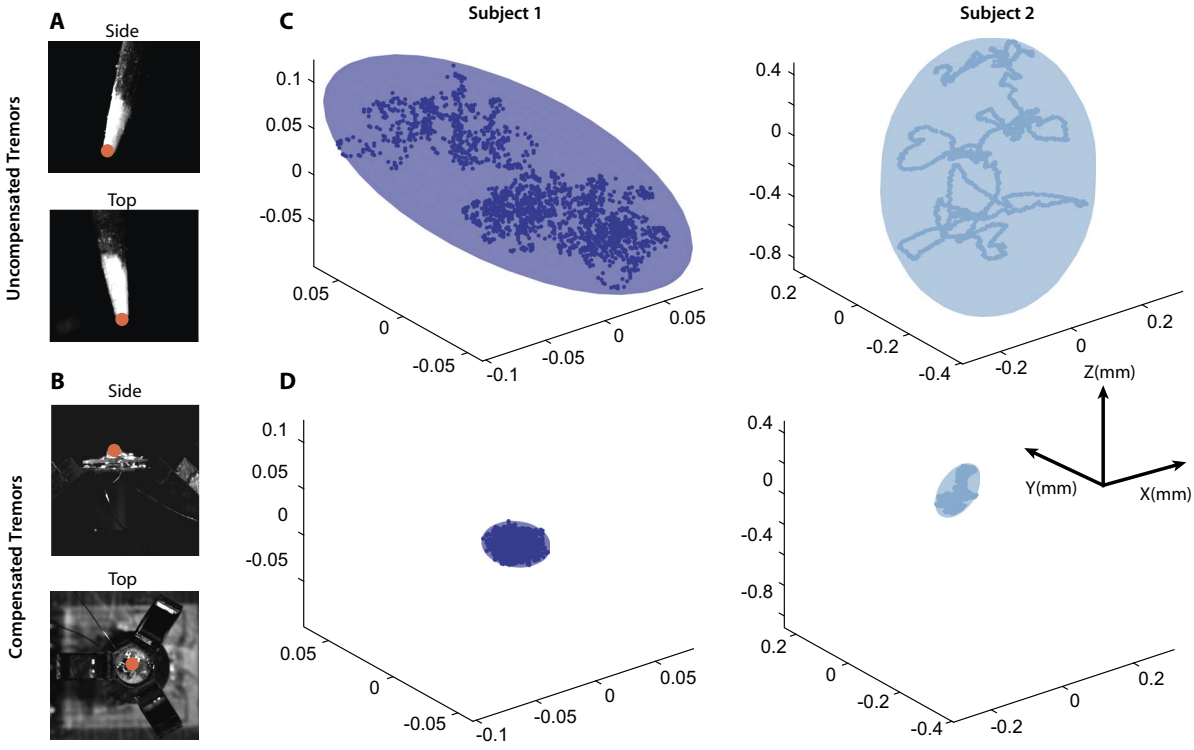

Fig. 7. Experimental results for tremor reduction. Orthogonal camera views used to record hand tremors (**A**) and milliDelta motion (**B**) are shown with a red circle denoting the tracked point. (**C**) Tremor data for two individuals are shown with bounding ellipsoids. The linear model was inverted offline to allow the milliDelta to track the measured tremors, and the tracking error is shown with bounding ellipsoids (**D**). The milliDelta was able to reduce hand tremor magnitudes by 81% RMS.

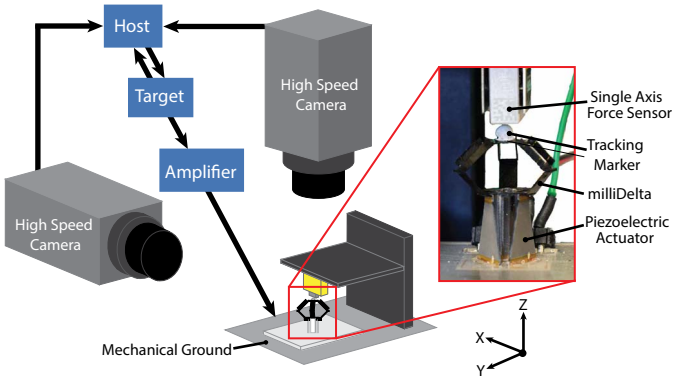

Fig. 8. Experimental setup for workspace, bandwidth, and force characterization of the milliDelta. Two orthogonal, synced, high-speed cameras were centered on the milliDelta. A reflective marker was placed on the output stage, and its position was tracked by using vision-based techniques. For force testing, a single-axis force sensor that obscured the top camera was positioned above the milliDelta. The cameras, force sensor, and milliDelta were controlled in real time by using MATLAB's xPC target system.

(Mathworks) and calibrated using the camera calibration toolbox for MATLAB to provide the 3D position of the milliDelta. The experimental setup (Fig. 8) was modified for the blocked force measurements as follows: A single-axis force sensor (Futek LSB200) was positioned above the milliDelta on a micropositioning stage (Thorlabs), and the high-speed cameras were not used.

Workspace

To determine the volume of the milliDelta's workspace, we actuated each arm individually with the other two arms fixed at their extreme positions (12 trials). In addition, pairs of arms were actuated together with the inactive arm fixed at its extreme positions (six trials). For each of the 18 actuation schemes tested, the actuators were driven by 100-V peak-to-peak, 2-Hz sinusoidal signals. Higher input voltages resulted in linkage collisions for certain actuation schemes. Eight cycles of data were recorded for each scheme at 50 frames per cycle (fpc), corresponding to 100 frames per second (fps).

Blocked force measurements

Blocked force was measured in the vertical direction by driving all three actuators with a 200-V peak-to-peak, 1-Hz sinusoidal signal. The force sensor was positioned directly above the milliDelta and was moved upward at increments of 500 μm until the output stage no longer contacts the sensor. Five cycles of force data were recorded at each height.

Frequency response

The frequency response was measured by exciting each arm with independently generated band-limited (200 Hz) white noise voltages with RMS amplitudes of ~5.5 V. The motion of the milliDelta was recorded at 4000 fps for 10 s.

Trajectory following

Desired actuator input deflections were generated by using the kinematic model for the three quasi-static (1 Hz) trajectories, and signal

amplitudes were selected to match these deflections. Data were recorded at 100 fps for five cycles. The estimated dynamic model was inverted to generate inputs for the 20-Hz star and 75-Hz circle. The motion of the milliDelta was recorded at 100 fpc (2000 fps) and 40 fpc (3000 fps), respectively, for five cycles.

Tremor compensation

The estimated dynamic model was inverted in a postprocessing step to allow the milliDelta to track the recorded hand tremors. The hand tremors and milliDelta motions were recorded at 400 fps for 8 s. Hand tremors were measured for three individuals holding a visual marker (toothpick), approximating the frequency and magnitude of tremors measured during microsurgery (*47*–*50*). The raw hand tremor position data were filtered by using an acausal second-order low-pass Butterworth filter with a cutoff frequency of 50 Hz before the inverse dynamics are calculated.

SUPPLEMENTARY MATERIALS

robotics.sciencemag.org/cgi/content/full/3/14/eaar3018/DC1
Fig. S1. Relevant linkage parameters for one arm of the milliDelta.
Fig. S2. Manufacturing process for the milliDelta.
Fig. S3. Singular value plot of the transfer function matrix as a function of frequency.
Table S1. Link length parameters of the milliDelta, piezoelectric bending actuator dimensions, and flexure stiffnesses.
Movie S1. High-frequency motion.
Movie S2. Trajectory following.
Movie S3. Tremor compensation.
Reference (*51*)

REFERENCES AND NOTES

1. M. Stock, K. Miller, Optimal kinematic design of spatial parallel manipulators: Application to linear delta robot. *J. Mech. Des. N. Y.* **125**, 292–301 (2003).
2. M. López, E. Castillo, G. García, A. Bashir, Delta robot: Inverse, direct, and intermediate Jacobians. *P. I. Mech. Eng. C J. Mec.* **220**, 103–109 (2006).
3. J.-P. Merlet, *Parallel Robots* (Springer Science & Business Media, 2006).
4. R. Clavel, Device for the Movement and Positioning of an Element in Space, U.S. Patent 4,976,582 (1990).
5. R. Clavel, Conception d'un robot parallèle rapide à 4 degrés de liberté, thesis, École polytechnique fédérale de Lausanne EPFL (1991).
6. L.-W. Tsai, *Robot Analysis: The Mechanics of Serial and Parallel Manipulators* (John Wiley & Sons, 1999).
7. L. Rey, R. Clavel, The Delta Parallel Robot, in *Parallel Kinematic Machines*, C. R. Boër, L. Molinari-Tosatti, K. S. Smith, Eds. (Springer, 1999), pp. 401–417.
8. F. Pierrot, C. Reynaud, A. Fournier, DELTA: A simple and efficient parallel robot. *Robotica* **8**, 105–109 (1990).
9. P. Vischer, R. Clavel, Kinematic calibration of the parallel Delta robot. *Robotica* **16**, 207–218 (1998).
10. P. Vischer, R. Clavel, Argos: A novel 3-DoF parallel wrist mechanism. *Int. J. Rob. Res.* **19**, 5–11 (2000).
11. J.-P. Merlet, Direct kinematics of parallel manipulators. *IEEE Trans. Robot. Autom.* **9**, 842–846 (1993).
12. T. Brogårdh, Present and future robot control development—An industrial perspective. *Annu. Rev. Control* **31**, 69–79 (2007).
13. E. Pernette, S. Henein, I. Magnani, R. Clavel, Design of parallel robots in microrobotics. *Robotica* **15**, 417–420 (1997).
14. T. Tanikawa, M. Ukiana, K. Morita, Y. Koseki, K. Ohba, K. Fujii, T. Arai, Design of 3-DOF parallel mechanism with thin plate for micro finger module in micro manipulation, in *IEEE/RSJ International Conference on Intelligent Robots and Systems* (IROS, 2002), pp. 1778-1783.
15. T. Tanikawa, T. Arai, Development of a micro-manipulation system having a two-fingered micro-hand. *IEEE Trans. Robot. Autom.* **15**, 152–162 (1999).
16. J. E. Correa, J. Toombs, N. Toombs, P. M. Ferreira, Laminated micro-machine: Design and fabrication of a flexure-based Delta robot. *J. Manuf. Process.* **24**, 370–375 (2016).
17. A. Codourey, S. Perroud, Y. Mussard, Miniature reconfigurable assembly line for small products, in *Precision Assembly Technologies for Mini and Micro Products*, S. Ratchev, Ed. (Springer Science & Business Media, 2006), pp. 193–200.
18. M. Salerno, A. Firouzeh, J. Paik, A low profile electromagnetic actuator design and model for an origami parallel platform. *J. Mech. Robot.* **9**, 041005 (2017).
19. S. Perroud, A. Codourey, Y. Mussard, PocketDelta: A miniature robot for micro-assembly, *Proc. 5th International Workshop on Microfactories* (2006), pp. 3–5.
20. A. M. Hoover, R. S. Fearing, Fast scale prototyping for folded millirobots, in *IEEE International Conference on Robotics and Automation* (IRCA, 2008), pp. 886-892.
21. C. D. Onal, R. J. Wood, D. Rus, Towards printable robotics: Origami-inspired planar fabrication of three-dimensional mechanisms, in *IEEE International Conference on Robotics and Automation* (ICRA, 2011), pp. 4608-4613.
22. J. P. Whitney, P. S. Sreetharan, K. Y. Ma, R. J. Wood, Pop-up book MEMS. *J. Micromech. Microeng.* **21**, 115021 (2011).
23. R. J. Wood, S. Avadhanula, R. Sahai, E. Steltz, R. S. Fearing, Microrobot design using fiber reinforced composites. *J. Mech. Des. N. Y.* **130**, 052304 (2008).
24. L. L. Howell, *Compliant Mechanisms* (John Wiley & Sons, 2001).
25. R. S. Fearing, Powering 3 dimensional microrobots: Power density limitations, Tutorial on Micro Mechatronics and Micro Robotics, in *IEEE International Conference on Robotics and Automation* (ICRA, 1998), pp. 98.
26. S. Russo, T. Ranzani, C. J. Walsh, R. J. Wood, An additive millimeter-scale fabrication method for soft biocompatible actuators and sensors. *Adv. Mater. Technol.* **2**, 1700135 (2017).
27. K. Jaeyoun, *Microscale Soft Robotics: Motivations, Progress, and Outlook* (Springer, 2017).
28. N. T. Jafferis, M. J. Smith, R. J. Wood, Design and manufacturing rules for maximizing the performance of polycrystalline piezoelectric bending actuators. *Smart Mater. Struct.* **24**, 065023 (2015).
29. K. R. Oldham, J. S. Pulskamp, R. G. Polcawich, M. Dubey, Thin-film PZT lateral actuators with extended stroke. *J. Microelectromech. Syst.* **17**, 890–899 (2008).
30. D. J. Cappelleri, M. I. Frecker, T. W. Simpson, A. Snyder, Design of a PZT bimorph actuator using a metamodel-based approach. *Int. J. Mach. Tool Manuf.* **33**, 193–208 (2002).
31. W. S. N. Trimmer, Microrobots and micromechanical systems. *Sensor. Actuator.* **19**, 267–287 (1989).
32. R. J. Wood, Liftoff of a 60mg flapping-wing MAV, in *IEEE/RSJ International Conference on Intelligent Robots and Systems* (IROS, 2007), pp. 1889–1894.
33. K. L. Hoffman, R. J. Wood, Towards a multi-segment ambulatory microrobot, in *IEEE International Conference on Robotics and Automation* (ICRA, 2010), pp. 1196–1202.
34. A. T. Baisch, O. Ozcan, B. Goldberg, D. Ithier, R. J. Wood, High speed locomotion for a quadrupedal microrobot. *Int. J. Rob. Res.* **33**, 1063–1082 (2014).
35. Adept Quattro s650H (Omron Adept Technologies Inc.), Adept Hornet 565 (Omron Adept Technologies Inc.), picKstar YS02N (Kawasaki Heavy Industries Ltd.), Pocket Delta Robot (Asyril SA), Tripod EXPT (Festo), and IRB 360 FlexPicker (ABB).
36. Y. Li, Q. Xu, Design and analysis of a totally decoupled flexure-based XY parallel micromanipulator. *IEEE Trans. Robot.* **25**, 645–657 (2009).
37. S. Yang, R. A. MacLachlan, C. N. Riviere, Manipulator design and operation of a six-degree-of-freedom handheld tremor-canceling microsurgical instrument. *IEEE/ASME Trans. Mechatron.* **20**, 761–772 (2015).
38. A. Üneri, M. A. Balicki, J. Handa, P. Gehlbach, R. H. Taylor, I. Iordachita, New steady-hand eye robot with micro-force sensing for vitreoretinal surgery. *Proc. IEEE RAS EMBS Int. Conf. Biomed. Robot. Biomechatron.* **2010**, 814–819 (2010).
39. Y. Noda, Y. Ida, S. Tanaka, T. Toyama, M. F. Roggia, Y. Tamaki, N. Sugita, M. Mitsuishi, T. Ueta, Impact of robotic assistance on precision of vitreoretinal surgical procedures. *PLOS ONE* **8**, e54116 (2013).
40. M.-O. Demaurex, The Delta robot within the industry, in *Parallel Kinematic Machines*, C. R. Boër, L. Molinari-Tosatti, K. S. Smith, Eds. (Springer, 1999), pp. 395–399.
41. D. M. Aukes, R. J. Wood, Algorithms for rapid development of inherently-manufacturable laminate devices, *ASME Conference on Smart Materials, Adaptive Structures and Intelligent Systems* (2014).
42. N. Doshi, B. Goldberg, R. Sahai, N. Jafferis, D. M. Aukes, R. J. Wood, Model driven design for flexure-based microrobots, in *IEEE/RSJ International Conference on Intelligent Robots and Systems* (IROS, 2015), pp. 4119–4126.
43. K. Y. Ma, P. Chirarattananon, R. J. Wood, Design and fabrication of an insect-scale flying robot for control autonomy, in *IEEE/RSJ International Conference on Intelligent Robots and Systems* (IROS, 2015), pp. 1558-1564.
44. P. S. Sreetharan, J. P. Whitney, M. D. Strauss, R. J. Wood, Monolithic fabrication of millimeter-scale machines. *J. Micromech. Microeng.* **22**, 055027 (2012).
45. P. K. Gupta, P. S. Jensen, E. de Juan Jr., Surgical forces and tactile perception during retinal microsurgery, in *International Conference on Medical Image Computing and Computer-Assisted Intervention* (MICCAI, 1999), pp. 1218-1225.
46. P. Van Overschee, B. L. De Moor, *Subspace identification for linear systems: Theory - Implementation - Applications* (Springer Science & Business Media, 2012).
47. C. N. Riviere, R. S. Rader, N. V. Thakor, Adaptive cancelling of physiological tremor for improved precision in microsurgery. *IEEE Trans. Biomed. Eng.* **45**, 839–846 (1998).

48. S. P. N. Singhy, C. N. Riviere, Physiological tremor amplitude during retinal microsurgery, in *Proceedings of the IEEE 28th Annual Northeast Bioengineering Conference*, pp. 171–172.
49. W. T. Ang, P. K. Pradeep, C. N. Riviere, Active tremor compensation in microsurgery, in *26th Annual International Conference of the IEEE Engineering in Medicine and Biology Society* (2004), pp. 2738-2741.
50. R. J. Elbe, W. C. Koller, *Tremor, Johns Hopkins Series in Contemporary Medicine and Public Health* (Johns Hopkins Univ. Press, 1990).
51. D. E. Kirk, *Optimal Control Theory: An Introduction* (Courier Corporation, 2012).

Acknowledgments: We thank M. Acer, B. Goldberg, E. Helbling, K. Jayaram, and all members of the Harvard Microrobotics Laboratory for their advice and assistance. **Funding:** This work is partially funded by the Wyss Institute for Biologically Inspired Engineering and a National Defense Science and Engineering Graduate Fellowship. In addition, the prototypes were enabled by equipment supported by the ARO DURIP program (award #W911NF-13-1-0311). **Author contributions:** F.Z.T., J.-s.K., and R.J.W. initiated the project. H.M., F.Z.T., and N.D. designed and conducted the research, and all authors contributed to the development of the project and preparation of the manuscript. **Competing interests:** The authors declare that they have no competing interests. **Data and materials availability:** Contact H.D.M. or F.Z.T. for materials and data requests.

Submitted 24 October 2017
Accepted 14 December 2017
Published 17 January 2018
10.1126/scirobotics.aar3018

Citation: H. McClintock, F. Z. Temel, N. Doshi, J.-s. Koh, R. J. Wood, The milliDelta: A high-bandwidth, high-precision, millimeter-scale Delta robot. *Sci. Robot.* **3**, eaar3018 (2018).

Science Robotics

The milliDelta: A high-bandwidth, high-precision, millimeter-scale Delta robot

Hayley McClintock, Fatma Zeynep Temel, Neel Doshi, Je-sung Koh, and Robert J. Wood

Sci. Robot. **3** (14), eaar3018. DOI: 10.1126/scirobotics.aar3018

Science Robotics (ISSN 2470-9476) is published by the American Association for the Advancement of Science. 1200 New York Avenue NW, Washington, DC 20005. The title *Science Robotics* is a registered trademark of AAAS.